RSC Advances

PAPER

View Article Online
View Journal | View Issue

Cite this: *RSC Adv.*, 2024, **14**, 8556

Preparation of anisotropic polyimide aerogels for thermal protection with outstanding flexible resilience using the freeze-drying method

Bing Xu, * Hongtan Liang, Jie Hu, Jing Shu, Lei Zhang, Guozhi Fan, Zhipeng Zhang, Zhen Wang and Dehua Pan

Polyimide aerogels (PIAs) not only possess excellent thermodynamic properties but also have a high porosity structure, making them an exceptional protective and thermal insulation material, and further broadening their application scope in aerospace and other cutting-edge fields. In this work, a series of anisotropic polyimide aerogels (3,3′,4,4′-biphenyltetracarboxylic dianhydride (S-BPDA), *p*-phenylenediamine (PDA), 4,4′-diaminodiphenyl ether (ODA)) with excellent properties were prepared. These PIAs were obtained by unidirectional freeze-drying and thermal amination of two different precursor solutions mixed in proportion. These PIAs possess an irregularly oval tubular structure, exhibiting pronounced anisotropy. (PIA-2 exhibits outstanding flexible resilience in the radial direction. It can still regain its original form after half an hour of compression by a universal testing machine, yet it cannot do so in the axial direction. The thermal diffusivity of PIA-5 in the radial direction at room temperature is as low as 0.067 $mm^2 s^{-1}$, and even at 200 °C, the thermal diffusivity is as low as 0.057 $mm^2 s^{-1}$. Meanwhile, the thermal diffusivity in the axial direction at room temperature is 0.11 $mm^2 s^{-1}$, surpassing the value of 0.106 $mm^2 s^{-1}$ of aerogels prepared from monomeric raw materials and dried under supercritical conditions). PIAs exhibit outstanding thermal stability (the axial strength and modulus retention of PIA-8 at 200 °C are as high as 52.63% and 44.82%), and its weight loss temperature of 5% is as high as 603 °C and it has a glass softening temperature of 387 °C. PIAs also demonstrate exceptional flame retardancy in imitation flame retardant experiments and exhibit outstanding thermal insulation performance when heated on a 150 °C heating plate for 10 minutes (the radial surface temperature of PIA-5 was only 49.9 °C). These anisotropic PIAs materials exhibit outstanding flexible resilience, and thermal protection performance, holding significant importance for their widespread adoption as thermal insulation materials in aerospace, high-precision electronic components, and other domains.

Received 24th January 2024
Accepted 4th March 2024

DOI: 10.1039/d4ra00625a

rsc.li/rsc-advances

1 Introduction

In recent years, the aerospace sector has seen rapid development, with an endless stream of diverse spacecraft emerging. During the development of spacecraft, researchers discovered that the search for a lightweight, thermally stable insulation material has become a pivotal factor.[1–10]

As early as the 1930s, American researcher Kistler pioneered the use of supercritical drying equipment, using ethanol as the drying medium under high-temperature and high-pressure conditions, successfully producing silica aerogels for the first time. Although the process for preparing aerogels was complex, the experimental cycle was long, and it was not rapidly promoted at that time due to harsh conditions such as high temperature and high pressure, the successful preparation of silica aerogels also set off an upsurge of aerogel research in the scientific and technological community, laying the foundation for the promotion and application of aerogels in the field of cutting-edge technology in the early stage.[11–15]

An aerogel is a solid gel material with gas of dispersion medium. It is currently recognized as the solid with the lowest density. It possesses a three-dimensional porous structure and combines outstanding properties such as low density, high specific surface area, high porosity, low thermal conductivity, and low dielectric constant. It demonstrates significant application potential in the aerospace and civil sectors.[16–18]

Aerogels are primarily prepared using the sol–gel method. First, a suitable solvent is chosen as the pore-forming agent. Then, the sol is used for dispersion. Following that, the gel is used for shaping and curing. Finally, the solvent within the pores is separated through drying, resulting in a complete porous aerogel material. The most critical step is drying process, primarily focused on preventing the surface tension of liquid

Hubei Provincial Engineering Technology Research Center of Agricultural and Sideline Resources, Chemical Engineering and Utilization, School of Chemistry and Environmental Engineering, Wuhan Polytechnic University, Wuhan 430023, China. E-mail: xubing200806@163.com

within aerogel pores from compromising their integrity after drying and separation. Currently, the most widely adopted drying techniques include atmospheric drying, supercritical drying, and vacuum freeze drying. Atmospheric drying requires minimal equipment, offers cost-effectiveness, and boasts high safety.[19–25] However, due to the inherent surface tension at the solid–liquid interface during atmospheric drying, there's a risk of the aerogel's internal structure collapsing and shrinking. To prevent damage to the aerogel's pore structure from additional forces during the drying process, researchers might enhance the material's internal structure or minimize such forces. This approach, however, might limit the control over other aerogel characteristics, and it also restricts the selection and preparation processes of materials. Moreover, replacing organic solvents and aging the gel could take more time, further limiting the use of the atmospheric drying method. Supercritical drying can effectively prevent the damage of liquid surface tension to the pore structure of aerogel, but its complex process and high operational cost hinder its widespread adoption. Currently, vacuum freeze-drying outperforms atmospheric drying in terms of efficacy and offers a more cost-effective operation compared to supercritical drying. It particularly excels in controlling the internal microstructure of aerogels, making it the optimal method for preparing aerogels with anisotropic microstructures.[26–30]

Compared with inorganic aerogels, organic polymer aerogels have the advantages of high mechanical properties, easy processing and low thermal conductivity. Polyimide (PI) is regarded as a star material in the field of polymer materials and is widely used in aerospace, high-precision electronic components, lightweight materials, and other fields due to its excellent mechanical properties, high heat resistance, and chemical stability. Polyimide aerogels (PIAs) combine the excellent properties of PI and aerogels, boasting both good thermodynamic properties and high porosity and mesoporous structure, rendering them an exceptional protective and thermal insulation material, and making the widespread application of aerogels in aerospace a reality. With the advancement of hypersonic aircraft, the nose cone of the aircraft experiences an extremely high temperature environment, necessitating thermal insulation materials with superior performance. The unique properties of anisotropic PIAs have gained favor among aerospace scientists and technicians, making them a potential replacement for lightweight, small-scale thermal insulation materials in the thermal insulation and protection layer.[31–42]

Ma *et al.*[1] prepared anisotropic PIAs using the freeze-drying method. During the pre-freezing process, the internal structure of PIAs was controlled through unidirectional heat transfer from an aluminum plate. The resulting PIAs exhibited high anisotropy and outstanding mechanical properties across a broad temperature range. Pei *et al.*[2] crafted polyimide molecular chains of varying stiffness and flexibility. Using water-soluble polyamide acid salts and freeze-drying techniques, they produced a range of polyimide aerogels boasting high flexibility and low density. However, many scholars tend to focus on the thermal insulation and mechanical properties, neglecting the flexible resilience of the material. Thermal insulation materials must possess excellent flexible resilience. This ensures that, when utilized as protective insulation materials, they can swiftly regain their complete internal structure, thereby maintaining superior thermal insulation performance.

Concurrently, the flexible resilience enhances the bond between the protective and thermal insulation materials and the protected body, preventing bonding defects that could compromise the thermal insulation protection. Therefore, the optimal approach is to utilize commercial raw materials and the cost-effective freeze-drying method to produce anisotropic polyimide aerogel insulation materials, characterized by excellent flexible resilience, and low thermal conductivity, to realize its comprehensive performance advantages in the manufacture of hypersonic vehicles. In this study, a series of anisotropic polyimide aerogels (using ODA, PDA and S-BPDA as raw materials respectively) with excellent properties were prepared. These PIAs were obtained by unidirectional freeze-drying and thermal amination of two different precursor solutions mixed in proportion. These PIAs possess an irregularly oval tubular structure, exhibiting pronounced anisotropy (PIA-2 exhibits outstanding flexible resilience in the radial direction. It can still regain its original form after half an hour of compression by a universal testing machine, yet it cannot do so in the axial direction. The thermal diffusivity of PIA-5 in the radial direction at room temperature is as low as 0.067 $mm^2\ s^{-1}$, and even at 200 °C, the thermal diffusivity is as low as 0.057 $mm^2\ s^{-1}$. Meanwhile, the thermal diffusivity in the axial direction at room temperature is 0.11 $mm^2\ s^{-1}$, surpassing the value of 0.106 $mm^2\ s^{-1}$ of aerogels prepared from monomeric raw materials and dried under supercritical conditions[3]). These PIAs exhibit outstanding thermal stability (the axial strength and modulus retention of PIA-8 at 200 °C are as high as 52.63% and 44.82%), and its weight loss temperature of 5% is as high as 603 °C and glass softening temperature of 387 °C. PIAs also demonstrate exceptional flame retardancy in imitation flame retardant experiments and exhibit outstanding thermal insulation performance when heated on a 150 °C heating plate for 10 minutes (the radial surface temperature of PIA-5 was only 49.9 °C). These anisotropic PIAs materials exhibit outstanding flexible resilience, and thermal protection performance, holding significant importance for their widespread adoption as thermal insulation materials in aerospace, high-precision electronic components, and other domains.

2 Experiment

2.1 Materials

The reagents used in this experiment include 3,3′,4,4′-biphenyltetracarboxylic dianhydride (S-BPDA, AR), *p*-phenylenediamine (PDA, AR), 4,4′-diaminodiphenyl ether (ODA, AR), *N*,*N*-dimethylacetamide (DMAc, AR), diethylamine (AR), which were purchased from Shanghai McLean Biochemical Technology Co., Ltd, and anhydrous ethanol (AR), which were purchased from Sinopharm Chemical Reagent Co., Ltd.

2.2 Synthesis of polyimide aerogels

First, weigh 0.065 mol (7.02 g) of PDA, place it into 2.69 mol (235.00 g) of DMAC solvent, gently shake and oscillate. Then

weigh 0.065 mol (19.12 g) of S-BPDA and continue to add it to the solution. Under a nitrogen atmosphere, stir the solution in an ice water bath for 12 hours to obtain a yellowish-brown viscous polyamide acid solution. Add deionized water to the polyamide acid solution, and the solution will quickly solidify into polyamide acid strip solid when it meets water. After crushing the strip solid, wash it with boiling water and boiling ethanol for three times respectively, and then place the polyamide acid powder in the vacuum oven at 80 °C for 12 hours to obtain light yellow polyamide acid A powder. Similarly, by replacing PDA with 0.065 mol (13.01 g) of ODA, a pale yellow polyamide acid B powder was obtained. These two types of polyamide acid powders were mixed in proportion. Polyamide acid mixed powders of varying masses were reacted with diethylamine aqueous solution to prepare polyamide acid salt solutions with solid contents ranging from 3% to 11%. The precursor polyamide acid salt solutions with varying solid contents were poured into copper mold bases and numbered for identification. The mold was then placed in a −70 °C cold trap for 5 hours of unidirectional pre-freezing. Following the pre-freezing molding process, the samples underwent vacuum freeze-drying for 48 hours, maintaining a system temperature below −60 °C and a pressure below 3 Pa. Subsequently, the samples were subjected to a programmed temperature rise in a high-temperature oven, with a rate of 1 °C minute^{-1}, reaching temperatures of 60 °C, 90 °C, 120 °C, 150 °C, 180 °C, 210 °C, 240 °C, 270 °C and 300 °C for one hour each, completing the thermal imidization of the aerogel. Samples with different solid contents are denoted as PIA-*x*, where *x* represents the solid content of the polyimide aerogel, unit is %.

2.3 Characterization

The infrared spectra of the samples were measured using a Fourier transform infrared spectroscopy (FT-IR) instrument (IS50, PerkinElmer, USA), with a resolution of 4 cm^{-1} and a scanning range of 4000 cm^{-1} to 400 cm^{-1}. Solid-state ^{13}C nuclear magnetic resonance (NMR) spectroscopy was tested using a Bruker Avance II400 spectrometer (II400, Bruker, Switzerland). Sample density was measured using an electronic densitometer (MH-300A, Shanghai Qigong Instrument Equipment Co., Ltd, China). The shrinkage of aerogel was determined by the ratio of the diameter of the sample after drying to that before drying. The morphology of aerogel was examined using a thermal field emission scanning electron microscope (JSM-7610FPlus, JEOL, Japan) at an accelerating voltage of 15 kV. Thermogravimetric analysis (TGA) and the glass transition temperature were determined using a DSC/TGA synchronous thermal analyzer SDTQ600 (Q600, TA Company, USA), with a heating rate of 10 °C min^{-1}. A dynamic mechanical analyzer (Q800, TA Company, USA) was employed for the high-temperature compression performance test, operating in compression mode, with a test range of 50–400 °C, a heating rate of 10 °C min^{-1}, and a frequency of 1 Hz. The ambient-temperature compression performance test was conducted using an electronic universal testing machine (HR-500, Guangdong Hairui Testing Instrument Co., Ltd, China) with a 1 kN sensor and a compression speed of 2 mm min^{-1}. The compression performance of aerogel was evaluated in accordance with the Chinese national standard GB/T 8813-2008. The flame retardancy test of aerogel materials was carried out in accordance with the Chinese national standard GB/T2408-2008. The dimensions of the cube samples were 15 mm in length and width, and 10 mm in thickness. The sample is held and fixed using tweezers, then subjected to a 10-second burn using a flame spray gun. Following the burn, the sample's morphology is observed and recorded. Subsequently, the sample is again subjected to a 10-second burn, after which the flame is extinguished and the sample's morphology is again observed and recorded. The sample is then removed for thickness measurement and analysis. The thermal diffusivity was measured using the HyperFlash Laser Thermal Conductivity Analyzer (LFA 467, Netzsch, Germany) over the temperature range of 25 to 300 °C, the prepared sample is a 10 × 10 × 1 mm rectangular square, which is a quadrilateral plane with a side

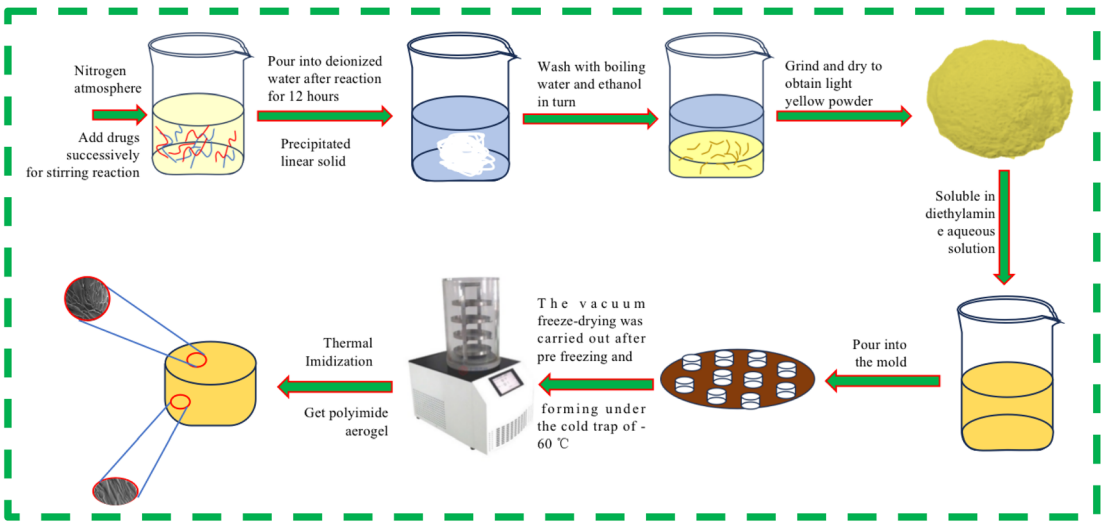

Fig. 1 Preparation process of polyimide aerogel samples.

length of 10 mm in the axial or radial direction and a thickness of 1 mm. The plane is crossed by graphite to prevent light transmission. The thermal imaging of the heating process was captured using an infrared thermal camera (FOC 326L, Shanghai Thermal Imaging Technology Co., Ltd, China). The aerogel sample was heated on a hot plate at 150 °C for 10 minutes, with the entire heating process being monitored by the thermal camera. The sample is a cube with a side length of 10 mm.

3 Result and discussion

3.1 Structural characterization of PIAs

The preparation procedures for PIAs and the fundamental principles of PI synthesis are illustrated in Fig. 1 and 2, respectively. First, different polyamide acid powders A and B are prepared. These two types of polyamide acid powders are then mixed in a specific ratio. Subsequently, they are reacted with a diethylamine solution to produce varying concentrations of PI precursor solutions. These solutions are then poured into molds with copper plates at the bottom. The copper plate's thermal conductivity at room temperature is 401 W (m^{-1} K^{-1}), significantly higher than that of aluminum as cited in ref. 1. The mold is then placed in a −70 °C cold trap for unidirectional pre-freezing to adjust its structure. Finally, PIAs are obtained through a vacuum freeze-drying process and a thermal imidization step.

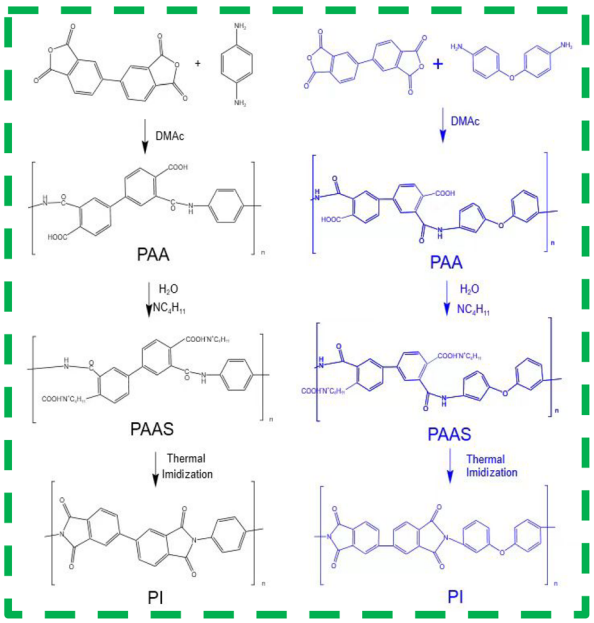

Fig. 2 Reaction principle of polyimide.

As shown in Fig. 3(a) FTIR, PIA samples exhibit a prominent characteristic absorption peak within the 1200–1350 cm^{-1} range. According to ref. 1 and 3, these peaks can be attributed to the absorption peaks generated by the vibration of C–N bonds in polyimide molecules. There are also strong characteristic absorption peaks within the 1400–1500 cm^{-1} range, which can be attributed to the N–H bond deformation vibration in the polyimide molecular chain. Similarly, there is a strong characteristic absorption peak within the 1500–1600 cm^{-1} range, which corresponds to the C=C bond vibration in the aromatic molecular ring of polyimide molecules. Furthermore, there are significant characteristic absorption peaks within the 1600–1800 cm^{-1} range, which can be attributed to the vibrational absorption peaks of carboxylic acid and imide bonds in the polyimide molecular skeleton. These characteristic peaks provide compelling evidence that the matrix synthetic material of aerogel is polyimide. To further confirm the identity of the aerogel collective, solid-state ^{13}C NMR spectroscopy was employed in this study. As shown in Fig. 3(b) ^{13}C NMR, the peak at 165 ppm can be attributed to the hydroxyl carbon on the imide group (C=O), while the peaks at 120–140 ppm can be attributed to the carbon atoms on the benzene ring of the polyimide molecule. The peak at 9 ppm can be attributed to the ether carbon atom.[3] These ^{13}C NMR results further confirm that the matrix synthetic material of aerogel is polyimide. The density and contraction rates of PIAs samples are illustrated in Fig. 4(a) and (b), respectively. As the solid concentration of the precursor solution increases, the density of the aerogel progressively rises, from 0.04 g cm^{-3} to 0.081 g cm^{-3}. PIA-2, with a density as low as 0.04 g cm^{-3}, exhibits notable

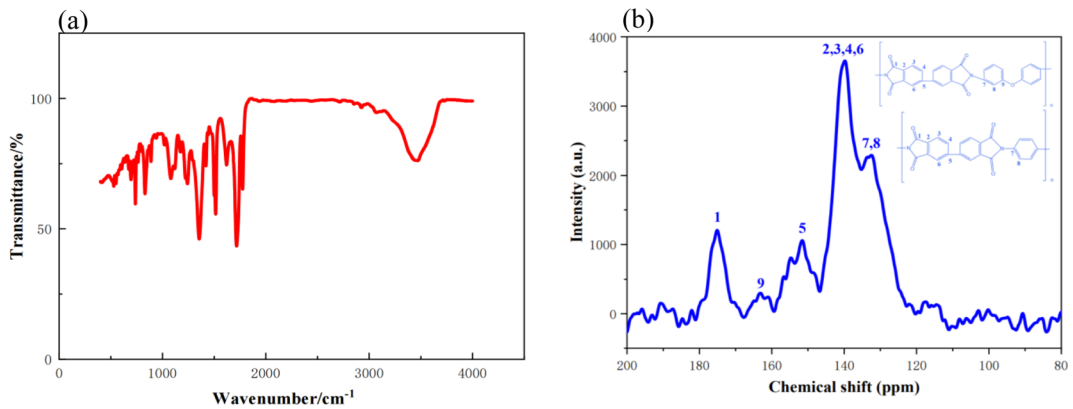

Fig. 3 FTIR (a) and ^{13}C NMR (b) spectra of PIA-3.5.

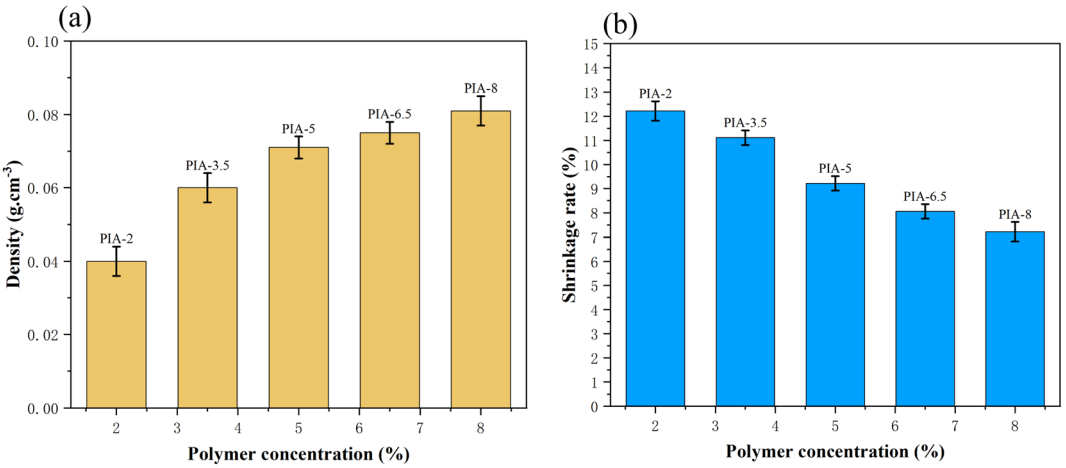

Fig. 4 Density and shrinkage of PIAs.

lightweight characteristics. The contraction rate of the aerogel decreases from 12.22% to 7.22% with the rising solid content. The primary reason for this is the increased solid content of the precursor, leading to more polymers precipitating during the phase separation process, thereby reducing the contraction rate of the aerogel. PIA-2 had a contraction rate of 12.22%, while PIA-8's was 7.22%.

The internal structure of PIAs samples along the axial and radial was observed by scanning electron microscope. The test results are shown in Fig. 5. From Fig. 5(a)–(f), in the axial

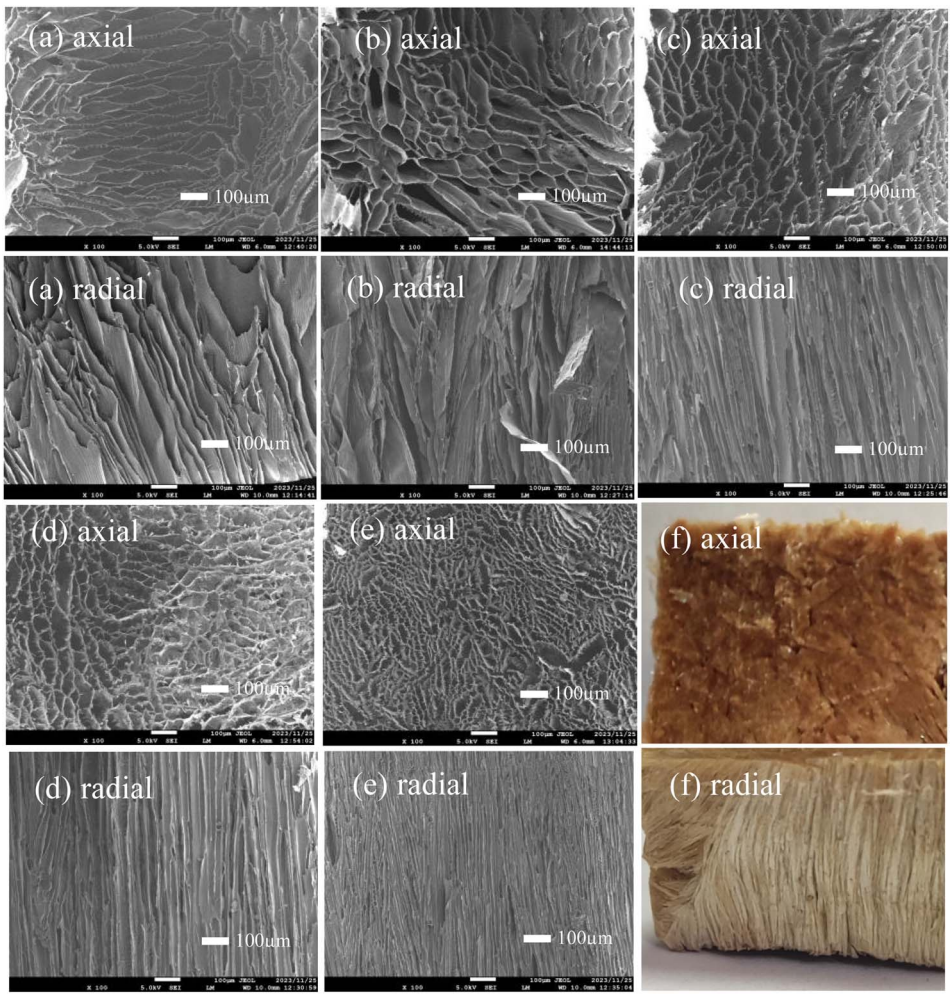

Fig. 5 SEM and physical photos of PIAs in both axial and radial: (a) PIA-2, (b) PIA-3.5, (c) PIA-5, (d) PIA-6.5, (e) PIA-8, (f) PIA-2.

direction, the pore shape of PIAs samples is irregular oval, and the pore size gradually decreases with the increase of solid content. According to the picture scale, the long axis size of pore ellipse of PIA-2 sample is greater than 100 μm, and the short axis length is about 50 μm. The major axis size of pore ellipse of PIA-8 sample is less than 50 μm, and the minor axis length is about 20 μm. This is mainly because when the current polymer solution is frozen at −70 °C, with the increase of polymer concentration, the polymer in the solution is more prone to phase separation and forms a more compact pore structure. Combined with the electron microscope images of the samples in the radial direction, it can be seen that PIAs are a porous material with quite obvious anisotropic structure, and the morphology of its pore structure is an irregular elliptical tubular pore structure. This is mainly because during unidirectional pre freezing, the solvent of the precursor solution crystallizes rapidly from bottom to top on the surface of the copper plate with rapid heat transfer, resulting in phase separation of the polymer, thus forming an aerogel skeleton with an irregular elliptical tubular pore structure. The experimental results show that the controllable anisotropic structure can be modulated by unidirectional pre freezing of copper plate heat transfer.

3.2 Thermal stability of PIAs

To evaluate the thermal stability of aerogel materials, TGA and DSC were employed for characterization. As illustrated in Fig. 6(a), under an air atmosphere, the temperature at which the sample loses 5% of its weight (T_d 5%) is 603 °C, and the temperature at which the sample loses 10% of its weight (T_d 10%) is 626 °C. These values are 48 °C and 41 °C higher, respectively, than those of PIAs synthesized from the rigid monomer PDA alone.[1] Conversely, Fig. 6(b) demonstrates that the glass transition temperature (T_g) of polyimide aerogel (PIA-5) reaches 387 °C, exhibiting a notable increase of 9 °C compared to the reported value of 379 °C in the reference sample.[1]

The results indicate that the PIAs samples, synthesized by physically mixing the polyamide acid salt solutions derived from rigid monomer PDA and flexible monomer ODA, exhibit superior thermal stability. The primary reason may be attributed to the intertwining and integration of rigid and flexible polyimide molecules, resulting in a more compact material binding.

3.3 Flexible resilience of PIAs

Thermal insulation protective materials must adhere well to the object they are protecting. In the protective structures of high-speed aircraft, the inner layer frequently employs aerogel thermal insulation materials as the final layer of thermal protection, while the outermost layer typically utilizes ablation-resistant ceramic composite materials. As the final layer of thermal insulation, it is essential for the material to harmoniously blend with both the outer composite layer and the protected internal structure. This necessitates aerogel materials to be not only lightweight and effective in thermal insulation but also possess adequate flexible resilience. Such materials, with their flexible resilience, can swiftly restore their internal structure upon exposure to external forces, thereby preserving their thermal insulation properties.

As illustrated in Fig. 7(a), the PIA-2 sample was briefly pressed by fingers in the axial direction, and the slide indicated 16 mm prior to the second pressing. Following the brief pressing, the slide's scale read 10 mm, indicating that the PIA-2 sample was compressed by 6 mm, leading to noticeable deformation. Upon release of the pressing finger, the PIA-2 sample rebounded, and the slide's scale returned to 16 mm, signifying that the PIA-2 has regained its original shape. The PIA-2 exhibits outstanding flexible resilience in the axial direction over a short time period. This suggests that by incorporating the flexible monomer ODA while maintaining a polyimide tubular framework with a low solid content, the framework can recover to its original shape after bending in a short time under external forces.

To further assess the flexible resilience of PIAs, the research group conducted comprehensive tests utilizing a universal testing machine. They subjected samples PIA-2, PIA-3.5, and

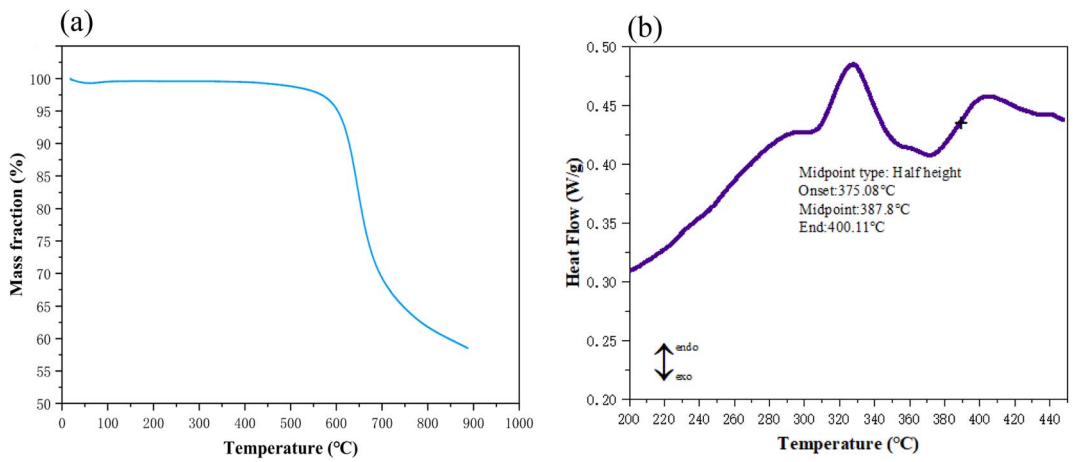

Fig. 6 TGA (a) and DSC (b) test curves of PIA-5 samples.

Fig. 7 PIAs compression rebound schematic diagram, (a) finger pressing in the axial direction of PIA-2, (b) PIAs radial compression test, (c) PIAs axial compression test.

PIA-5 to a 30-minute compression test in both axial and radial, as illustrated in Fig. 7(b) and (c). The test results revealed that, in the radial direction, as the solid content increased, the flexible resilience performance gradually diminished. Despite undergoing a 30-minute compression, PIA-5 still exhibited some flexible resilience but was unable to regain its original shape, displaying significant deformation. Meanwhile, sample PIA-2 maintained outstanding flexible resilience. In the axial direction, after a 30-minute compression, all three samples failed to rebound to their original shape. This was primarily due to the internal structure of PIAs. As seen from SEM images, PIAs' internal structure consists of irregular elliptical, tubular-shaped pores. Compression in the axial direction results in the axial compression of the tubular structure, which can maintain its elasticity by twisting. However, prolonged compression leads to the collapse of the tubular structure, thereby destroying its internal structure and causing a loss of flexible resilience. In the radial direction, when compressed along the elliptical's tubular radial direction, the elliptical structure enhances the material's flexible resilience performance. After a brief compression, the

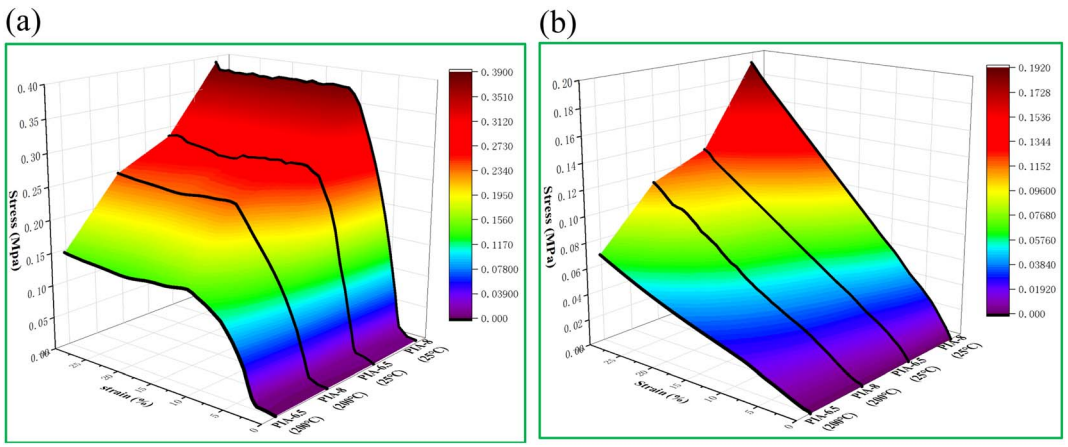

Fig. 8 Compression performance of PIAs at different temperatures, (a) axial of PIAs, (b) radial of PIAs.

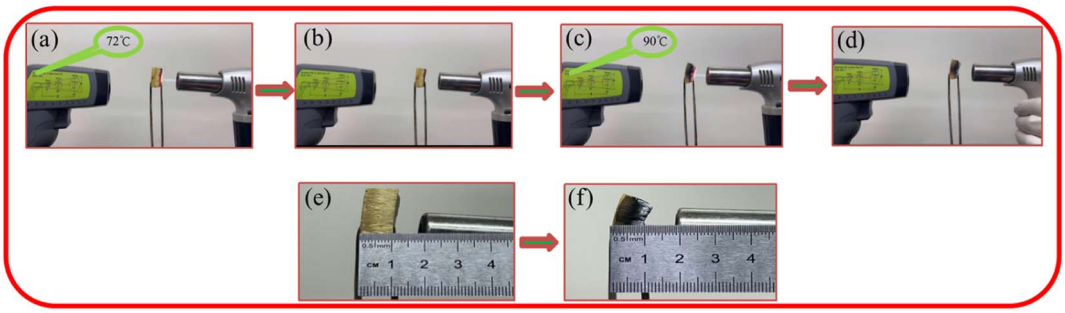

Fig. 9 Flame retardant experiment of PIA-5 sample. (a) During the initial ten-second burning phase. (b) After ten-second burn, stop burning. (c) During the second ten-second burning phase. (d) After the second ten-second burn, stop the burn. (e and f) Dimensional changes before and after burning phase.

Table 1 Physical properties in different directions of PIAs

	Stress (MPa)				Modulus (MPa)					
Solids (%)	25 °C axial	25 °C radial	200 °C axial	200 °C radial	25 °C axial	25 °C radial	200 °C axial	200 °C radial	Density (g cm^{-3})	Shrinkage rate (%)
2	—	—	—	—	—	—	—	—	0.040	12.22
3.5	—	—	—	—	—	—	—	—	0.060	11.11
5	—	—	—	—	—	—	—	—	0.071	9.22
6.5	0.28	0.040	0.13	0.020	3.16	0.40	1.50	0.20	0.075	8.06
8	0.38	0.060	0.20	0.030	3.57	0.60	1.60	0.30	0.081	7.22

flexible resilience performance of the sample gradually decreased with an increase in solid content. PIA-2, however, exhibited outstanding flexible resilience, maintaining its original shape. Therefore, PIAs' flexible resilience is superior in the radial direction to the axial direction, and the performance gradually decreases with an increase in solid content.

3.4 Mechanical properties of PIAs at different temperatures

The compressive properties of PIA-6.5 and PIA-8 samples were tested in both axial (Fig. 8(a)) and radial (Fig. 8(b)). The test results revealed that PIAs exhibited pronounced anisotropy. With increasing temperature, both the strength and modulus of the aerogel decreased in both axial and radial. This is attributed to the heightened mobility of the segments at elevated temperatures, which makes the aerogels more susceptible to deformation upon application of external forces. While high temperatures do reduce the mechanical properties of the material, the prepared samples maintained good modulus and strength even at 200 °C. The strength and modulus of PIA-6.5 in the axial direction reached 0.28 MPa and 3.16 MPa at room temperature, and those of PIA-8 reached 0.38 MPa and 3.57 MPa. The strength and

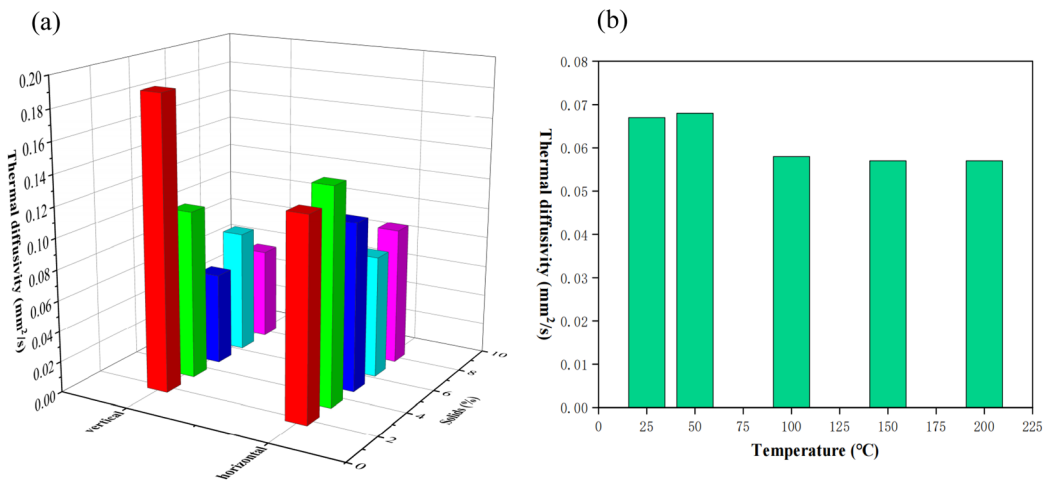

Fig. 10 Thermal insulation performance of PIAs. (a) Thermal diffusivity of PIAs in various directions. (b) Thermal diffusivity of PIA-8 under temperatures of 25, 50, 100, 150 and 200 °C.

modulus of PIA-6.5 at 200 °C were 0.13 MPa and 1.50 MPa, and those of PIA-8 were 0.20 MPa and 1.60 MPa (Table 1). Consequently, the strength and modulus of PIAs were higher in the axial direction than in the radial direction. This is primarily because the aerogel's internal structure is an irregular elliptical tubular pore, which offers robust bearing capacity in the axial direction. In contrast, the unstable elliptical structure leads to inferior bearing capacity in the radial direction. Furthermore, at 200 °C, the strength and modulus retention of PIA-8 in the axial direction reached 52.63% and 44.82%, outperforming the values reported in literature at 170 °C (56.80% and 34.6%).[1]

3.5 Flame retardant performance of PIAs

As shown in Fig. 9, the flame retardancy test was conducted on the PIA-5 sample. The TORCH400 butane flame spray gun was used to incinerate the PIA-5 sample. During the initial ten-second burning phase, the temperature measured by the thermometer was only 72 °C (Fig. 9(a)), while the butane spray gun's flame temperature could reach 1200–1300 °C. After ten seconds, the burning abruptly ceased, and the sample remained free of combustible flames, achieving automatic fire extinguishment without melting or dripping (Fig. 9(b)). Upon initiating a second ignition, the temperature on the reverse side of the PIA-5 sample's burning surface rose to 90 °C (Fig. 9(c)), indicating a reduction in sample thickness. After ten seconds, the burning ceased abruptly, and the sample remained free of combustible flames, achieving automatic fire extinguishment without melting or dripping (Fig. 9(d)). By comparing the dimensions of the sample before burning with those after two burning sessions, it was observed that less than 50% of the sample's thickness was incinerated, and the incinerated portion

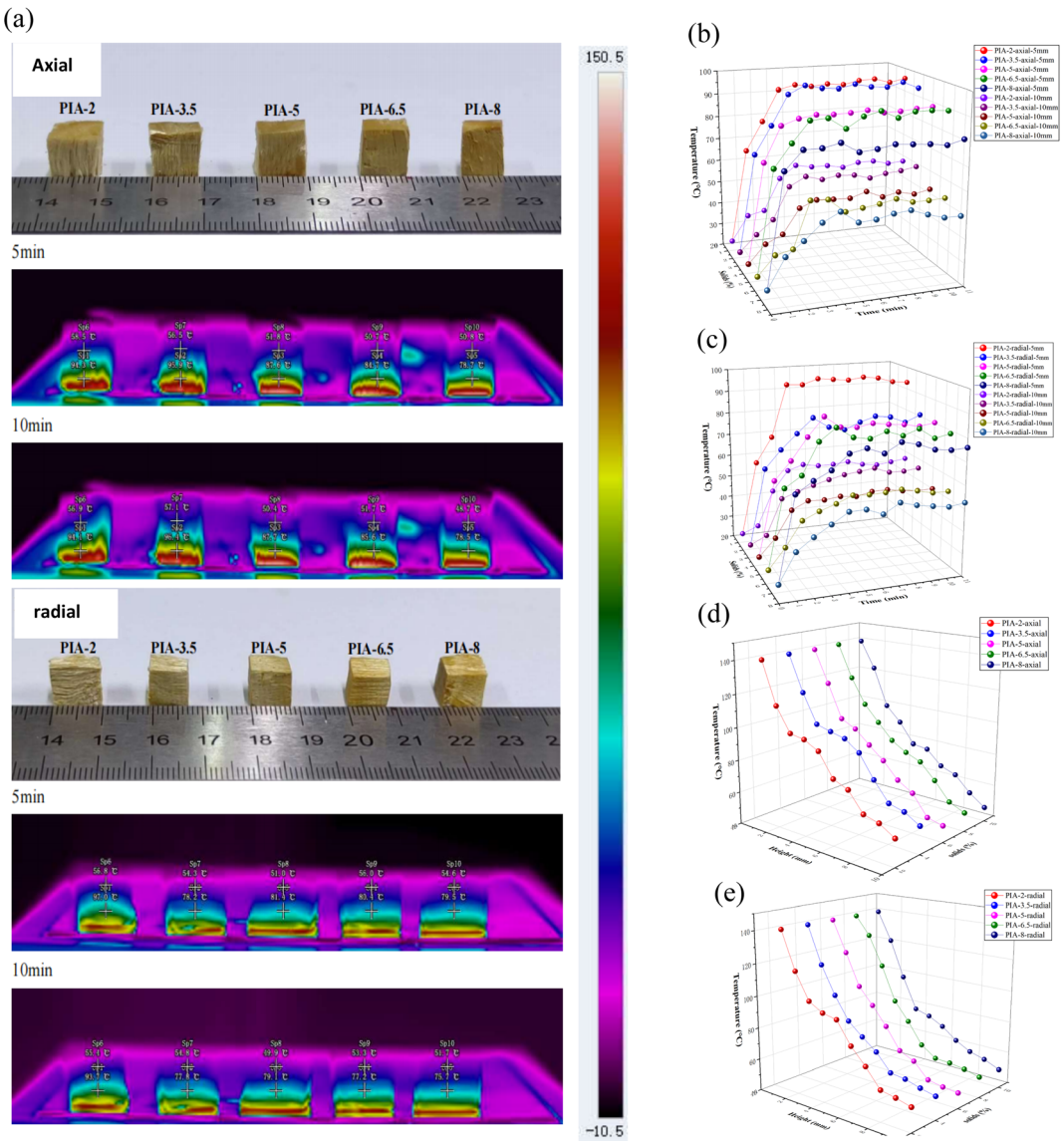

Fig. 11 (a) Infrared thermograms of PIAs heated on a high temperature plate at 150 °C for 5 minutes and 10 minutes, (b) temperature *versus* time curve of PIAs at 5 mm and 10 mm in axial direction, (c) temperature *versus* time curve of PIAs at 5 mm and 10 mm in radial direction, (d) temperature *versus* hight curve of PIAs in axial direction, (e) temperature *versus* hight curve of PIAs in radial direction.

transformed into amorphous carbon, still adhering to the sample (Fig. 9(d) and (e)). This suggests that the aerogel network formed by PIAs aerogel effectively suppresses the spread of flames. The prepared PIAs materials demonstrate not only outstanding thermal insulation properties but also exceptional flame retardancy.

3.6 Thermal insulation performance of PIAs

To characterize the thermal conductivity of PIAs, we utilized a laser flash thermal conductivity meter to measure their thermal diffusivity. Thermal diffusivity represents the rate at which temperature fluctuations are transmitted from one location to another within an object. For heat transfer, thermal diffusivity exhibits a more sensitive response than thermal conductivity. As shown in Fig. 10(a), at room temperature of 25 °C, with the increase of solid content, the thermal diffusivity first decreases and then increases in both axial and radial. The initial decrease in the thermal diffusivity is primarily attributed to the increased polymer matrix, which elevates the density of PIAs's framework, leading to a gradual reduction in material pore size. However, with an increase in the number of pore sizes, the increased amount of gas within the aerogel results in reduced gas mobility within the pore, leading to a decrease in PIAs's thermal diffusivity and an enhancement in its thermal insulation performance. Following the initial decrease, there is a subsequent increase in both directions of PIAs with an increase in solid content. The primary reason for this trend might be when the solid content increases to a certain extent, the dominant trend of heat transfer shifts from the influence of gas heat conduction in pores to the influence of the skeleton material's heat conduction. Concurrently, the radial thermal diffusivity is consistently lower than that of the axial. This is primarily due to the elliptical tubular polymer framework dominating the axial heat conduction, whereas the radial heat conduction is primarily driven by the gas within the elliptical tube. PIA-5 exhibits the best thermal insulation performance in the radial direction, with its thermal diffusivity reaching a minimum of 0.067 $mm^2 s^{-1}$ (0.11 $mm^2 s^{-1}$ in the axial direction). Fig. 10(b) presents a histogram of the thermal diffusivity of PIA-5 at various temperatures in the radial direction. These findings reveal that as the temperature increases from room temperature to 200 °C, the thermal diffusivity of PIAs initially decreases slightly and then remains stable, reaching a minimum of 0.057 $mm^2 s^{-1}$ at 200 °C. PIA-5 maintains its outstanding thermal insulation performance even at elevated temperatures, outperforming PIAs produced from the flexible monomer ODA using a supercritical device (0.106 $mm^2 s^{-1}$).[3]

The thermal insulation performance of PIAs was verified through infrared thermal imaging (as shown in Fig. 11). It can be observed from Fig. 11(a) that samples with varying solid contents are positioned on the heating plate in both axial and radial orientations for a 10-minute heating process at 150 °C. Throughout this process, an infrared camera monitors the temperature changes of the aerogel material. The temperature of the same aerogel section rises over time. After approximately 5 minutes, the lowest temperature observed on the axial surface of PIAs (at a distance of 10 mm) is 51.8 °C (PIA-5 axial), while the lowest temperature on the radial surface is 51.0 °C (PIA-5 radial). After 10 minutes, the lowest temperature on the axial surface is 50.4 °C (PIA-5 axial), and the lowest temperature on the radial surface is 49.9 °C (PIA-5 radial). As shown in Fig. 11(b) and (c), with the passage of time, the temperature of the aerogel sample increases at both the 5 mm and 10 mm points on both the axial and radial. After approximately 5 to 6 minutes, the temperature stabilizes. After a 10-minute heating process in both axial and radial orientations, the temperature of the material decreases as it rises in height, as depicted in Fig. 11(d) and (e).

The infrared thermal imaging experiment, utilizing a hot plate, once again confirmed the outstanding thermal insulation properties of the PIAs material. Furthermore, the radial thermal insulation of the PIAs material outperforms its axial counterpart, with the PIA-5 sample demonstrating the best performance in this regard. This further supports the thermal diffusivity test results of the aforementioned samples.

4 Conclusion

In summary, a series of anisotropic polyimide aerogels (S-BPDA, PDA, and ODA) with excellent properties were prepared. These PIAs were obtained by unidirectional freeze-drying and thermal amination of two different precursor solutions mixed in proportion. These PIAs possess an irregularly oval tubular structure, exhibiting pronounced anisotropy, PIA-2 exhibits outstanding flexible resilience in the radial direction. It can still regain its original form after half an hour of compression by a universal testing machine, yet it cannot do so in the axial direction. The thermal diffusivity of PIA-5 in the radial direction at room temperature is as low as 0.067 $mm^2 s^{-1}$, and even at 200 °C, the thermal diffusivity is as low as 0.057 $mm^2 s^{-1}$. Meanwhile, the thermal diffusivity in the axial direction at room temperature is 0.11 $mm^2 s^{-1}$, surpassing the value of 0.106 $mm^2 s^{-1}$ of aerogels prepared from monomeric raw materials and dried under supercritical conditions. PIAs exhibit outstanding thermal stability (the axial strength and modulus retention of PIA-8 at 200 °C are as high as 52.63% and 44.82%, and its weight loss temperature of 5% is as high as 603 °C and glass softening temperature of 387 °C). PIAs also demonstrate exceptional flame retardancy in imitation flame retardant experiments and exhibit outstanding thermal insulation performance when heated on a 150 °C heating plate for 10 minutes (the radial surface temperature of PIA-5 was only 49.9 °C). These anisotropic PIAs materials exhibit outstanding flexible resilience, and thermal protection performance, holding significant importance for their widespread adoption as thermal insulation materials in aerospace, high-precision electronic components, and other domains.

Conflicts of interest

There are no conflicts of interest to declare.

Acknowledgements

This research was supported by the financial assistance provided by the Key Project of the Scientific Research Program

of the Hubei Provincial Department of Education (D20201602) and the Hubei Natural Science Foundation (2023AFB385).

References

1 S. Ma, C. Wang, B. Cong, H. Zhou, X. Zhao, C. Chen, D. Wang and C. Qu, *Chem. Eng. J.*, 2022, **431**, 13047.
2 D. Pei, B. Lv, J. Wang, S. Qi, G. Tian and D. Wu, *Soft Mater.*, 2021, **19**, 50–55.
3 B. Xu, Z. Zhang, H. Liang, J. Hu, L. Chen, Z. Wang, B. Chai and G. Fan, *High Perform. Polym.*, 2023, 1–10.
4 M. Meador, E. MAlow, R. Silva, S. Wright, D. Quade, S. Vivod, H. Guo and J. Guo, *ACS Appl. Polym. Mater.*, 2012, **4**, 536–544.
5 T. Zhang, J. Yang, K. Wang and Y. Jiang, *J. Porous Mater.*, 2017, **24**, 1353–1362.
6 M. Fan, F. Gai, Y. Cao, Z. Zhao, Y. Ao, Y. Liu and Q. Huo, *J. Solid State Chem.*, 2019, **269**, 507–512.
7 Y. Lu and M. Zhan, *J. Polym. Sci., Part B: Polym. Phys.*, 2005, **43**, 3621–3627.
8 J. Kim, J. Lee and T. Song, *Int. J. Heat Mass Transfer*, 2012, **55**, 5343–5349.
9 Y. Zhuang, J. Seong and Y. Lee, *Prog. Polym. Sci.*, 2019, **35**, 88–92.
10 K. Qin, P. Cleo and M. Francisco, *J. Mater. Chem. B*, 2021, **9**, 889–907.
11 Z. Jaafar, B. Quelennec, C. Moreau, D. Lourdin, J. E. Maigret, B. Pontoire, A. D'orlando, T. Coradin, B. Duchemin, F. M. Fernandes and B. Cathala, *Carbohydr. Polym.*, 2020, **247**, 116642.
12 Z. Zhu, H. Yao, J. Dong, Z. Qian, W. Dong and D. Long, *Carbon*, 2018, **144**, 24–31.
13 J. Zhu, F. Zhao, R. Xiong, T. Peng and C. Jiang, *Composites, Part A*, 2020, **138**, 106040.
14 Y. Zhang, Q. Shen, X. Li, H. Xie and C. Nie, *RSC Adv.*, 2020, **10**, 42297–42304.
15 W. Wang, Y. Zhao, W. Yan, S. Cui, X. Wu and H. Suo, *J. Porous Mater.*, 2021, **28**, 703–710.
16 S. Zhang, J. Feng, J. Feng, Y. Jiang and F. Ding, *Appl. Surf. Sci.*, 2018, **440**, 873–879.
17 M. Gao, H. Kang, Z. Chen, E. Guo, Y. Fu, Y. Xu and T. Wang, *J. Alloys Compd.*, 2020, **818**, 153310.
18 A. Lamy-Mendes, R. Silva and L. Duraes, *J. Mater. Chem. A*, 2018, **6**, 1340–1369.
19 M. McEntee, W. Gordon, A. Balboa, D. Delia, C. Pit-man, A. Pennington, D. Rolison, J. Pietron and P. DeSario, *ACS Appl. Nano Mater.*, 2020, **3**, 3503–3512.
20 Y. Chen, S. Yang, D. Fan, G. Li and S. Wang, *J. Mater. Chem. A*, 2019, **7**, 12878–12886.
21 X. Zhang, H. Wang, Z. Cai, N. Yan, M. Liu and Y. Yu, *ACS Sustainable Chem. Eng.*, 2019, **7**, 332–340.
22 C. Liang and Z. Wang, *Chem. Eng. J.*, 2019, **373**, 598–605.
23 X. Zhang, W. Li, P. Song, B. You and G. Sun, *Chem. Eng. J.*, 2020, **381**, 122784.
24 R. Liu, X. Dong, S. Xie, T. Jia, Y. Xue, J. Liu, W. Jing and A. Guo, *Chem. Eng. J.*, 2019, **360**, 464–472.
25 J. Xiao, W. Lv and Y. Hu, *Chem. Eng. J.*, 2018, **338**, 202–210.
26 L. Ya, L. Yang, W. Choi, S. Chae, J. Lee, B. Kim, M. Park and H. Y. Kim, *J. Mater. Chem. A*, 2017, **5**, 2664–2672.
27 L. Hu, C. Xiao, Z. Yan, Z. Dian, Z. Ye, W. Chun, P. Cao, L. Chun and S. Chang, *Adv. Funct. Mater.*, 2021, **31**, 2008006.
28 F. Feng, T. Wei and W. Zhong, *Adv. Mater.*, 2016, **28**, 4283–4305.
29 S. Ghaffari, M. Aliofkhazraei, G. Darband, A. Zakeri and E. Ahmadi, *Surf. Interfaces*, 2019, **17**, 100340.
30 S. Ying, L. Da, W. Lan, Z. Yu, L. Feng, W. Hui, D. Bing and L. Qing, *ACS Appl. Mater. Interfaces*, 2021, **13**, 20489–20500.
31 M. Alipour, V. Gupta, M. Massoudinejad, S. Motahari and S. M. Zarandi, *Int. J. Environ. Anal. Chem.*, 2023, **103**, 8091–8109.
32 K. James, B. Amin and A. Bishnu, *Int. J. Biol. Macromol.*, 2023, **257**, 128478.
33 G. Cavallaro, G. Lazzara, E. Rozhina, S. Konnova, M. Kryuchkova, N. Khaertdinov and R. Fakhrullin, *RSC Adv.*, 2019, **9**, 40553–40564.
34 H. Guo, O. S. Dewey, L. S. McCorkle, M. A. B. Meador and M. Pasquali, *ACS Appl. Mater. Interfaces*, 2019, **1**, 1680–1688.
35 Z. Si, H. Xing, F. Jun, Q. Fang, E. Dian, J. Yong, L. Liang, X. Shi and F. Jian, *Cellulose*, 2020, **27**, 1–10.
36 Z. Xin, Y. Xi, W. Xin, C. Wei, G. Si, Z. Jing, L. Ben and L. Xiao, *Appl. Surf. Sci.*, 2020, **502**, 144187.
37 Z. Long, M. Cong, X. Fan, C. Shan and L. Zhao, *Cellulose*, 2020, **27**, 7677–7689.
38 C. Xiao, L. Hu, Z. Yan, Z. Yue, L. Xian, M. Li, G. Zhan and S. Chang, *ACS Appl. Mater. Interfaces*, 2019, **11**, 42594–42606.
39 C. Simón-Herrero, C. Xiao, M. L. Ortiz, A. Romero and L. Sánchez-Silva, *J. Mater. Res. Technol.*, 2019, **8**, 2638–2648.
40 L. Bo, J. Sheng, Y. Shu, C. Ying, T. Xiang, W. Xiao, Z. Ya, S. Xiao and C. Shen, *J. Sol-Gel Sci. Technol.*, 2018, **88**, 386–394.
41 M. Hao, J. Xin, M. M. A. Babin, G. Hai, T. Lih and G. Shao, *ACS Appl. Mater. Interfaces*, 2018, **10**, 30596–30606.
42 W. You, J. Dan, L. Yang, Z. Hui, W. Hao, S. Cheng, W. Yi, C. Zheng and G. Bin, *Polym. Test.*, 2020, **85**, 106405.